Article

Nafion-Immobilized Functionalized MWCNT-based Electrochemical Immunosensor for Aflatoxin B$_1$ Detection

Kai Deng,$^{\parallel}$ Yining Zhang,$^{\parallel}$ Hang Xiao, Yujiao Hou, Qingbin Xu, Ying Li, Weijun Kong, and Li Ma*

Read Online

ACCESS | Metrics & More | Article Recommendations

ABSTRACT: The ubiquitous aflatoxin B$_1$ (AFB$_1$) contamination in foods and other complex matrices has brought great challenges for onsite monitoring. In this study, an ultrasensitive Nafion-immobilized functionalized multiwalled carbon nanotube (MWCNT)-based electrochemical (EC) immunosensor was developed for trace AFB$_1$ detection. The introduced Nafion film could steadily stabilize functionalized MWCNTs with uniform distribution and tiling on the surface of a Au electrode. Functionalized MWCNTs with a large specific surface area, numerous active sites to couple with abundant anti-AFB$_1$ monoclonal antibodies (mAbs), and high conductivity served as the signal amplifier for remarkably enhancing the sensing performance of the immunosensor. In the presence of AFB$_1$, it was specifically captured by mAbs to reduce the amplified current signals, which were recorded by differential pulse voltammetry for the accurate quantitation of AFB$_1$. Because of the synergistic effects of Nafion on the stabilization of functionalized MWCNTs as signal enhancers, the developed EC immunosensor exhibited an extremely high selectivity, excellent sensitivity with a limit of detection as low as 0.021 ng/mL, and a wide dynamic range of 0.05−100 ng/mL, besides fascinating merits of easy construction, low cost, good stability in 7 days, and good reusability. The anti-interference ability of the immunosensor was verified against three other mycotoxins, and the practicability and accuracy were confirmed by measuring AFB$_1$ in fortified malt, lotus seed, and hirudo samples with a satisfactory recovery of 92.08−104.62%. This novel immunosensing platform could be extended to detect more mycotoxins in complex matrices to ensure food safety.
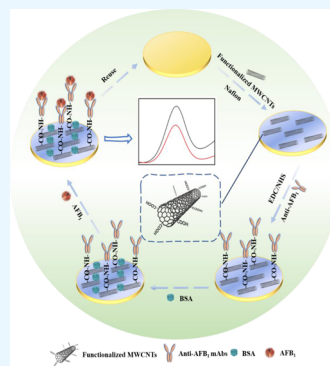
INTRODUCTION

Aflatoxins are mainly produced by some fungal strains such as *Aspergillus flavus* and *Aspergillus parasiticus* under humid and hot conditions,[1,2] which have been regarded as the most toxic mycotoxins in nature.[3,4] Of them, aflatoxin B$_1$ (AFB$_1$) is extremely toxic, with the characteristics of accumulation and concealment, and is usually found in foods, feedstuffs, and traditional Chinese medicines (TCMs),[5−8] thus accumulating in the kidney and liver of the human body to cause growth disorders, fibrous lesions, and fibrous tissue proliferation.[9−11] AFB$_1$ has been classified as a group IA carcinogen[12−14] and is strictly limited in food and agricultural products in the world.[15] Thus, there is great urgency and necessity for reliable techniques to monitor AFB$_1$ at trace levels in diverse complex matrices.

At present, many traditional strategies have been proposed for AFB$_1$ detection,[16−20] exhibiting fascinating advantages, including rapid analysis and high selectivity. Nevertheless, these methods rely on expensive and bulky instruments and professional operators, exhibit low detection ability, or easily cause false-positive results, making them unable to quickly and accurately monitor a large number of real samples. To overcome these limitations, a variety of biosensors have been constructed as candidates for measuring trace AFB$_1$. Among

them, electrochemical (EC) immunosensors have attracted increasing interest in trace analysis in different fields.[21,22]

Benefiting from the special recognition and strong binding ability between an antigen (Ag) and antibody (Ab), electrochemical immunosensors, by immobilizing Ab or complete Ag on sensing substrates such as Au electrodes, allow highly specific and sensitive detection of targets at extremely low levels in complex samples.[23] The whole detection process is fast, with low time and reagent consumption, and the Au working electrode is simple, reusable, and easy to carry for in situ or automatic detection.[24,25] More importantly, the complex sample pretreatment, expensive equipment and daily maintenance, and pollution of organic reagents are avoided. In addition, compared with optical signal-based methods, the color interferences from the sample extract are eliminated in the EC sensing to achieve a wider detection range. Because of
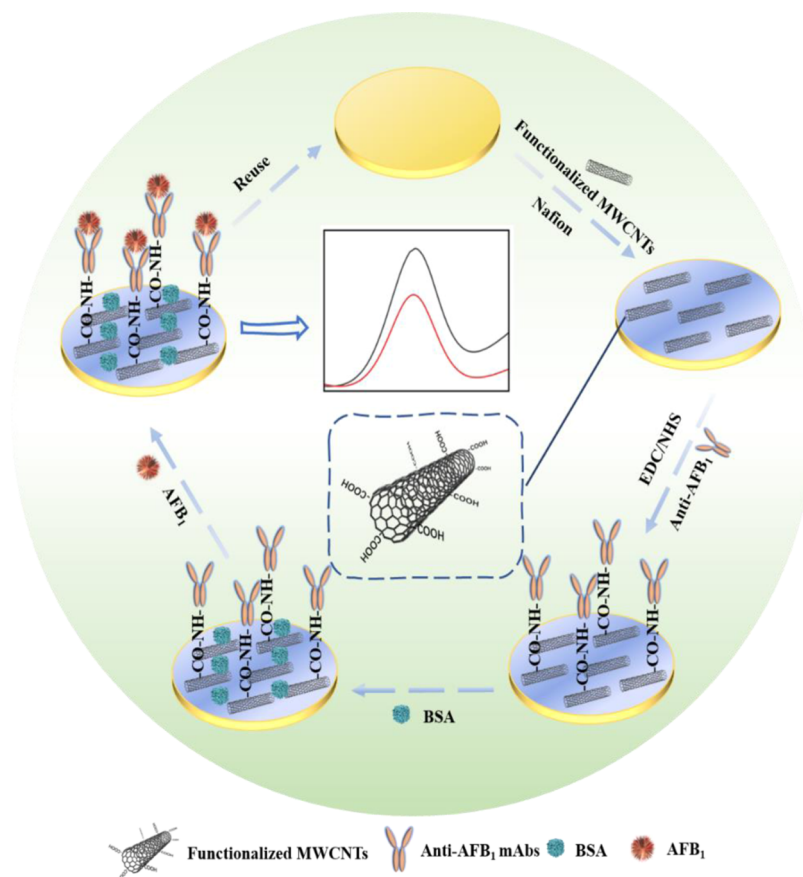
Scheme 1. Illustration of a Highly Sensitive Functionalized MWCNT-Based EC Immunosensor for AFB$_1$ Detection

Functionalized MWCNTs   Anti-AFB$_1$ mAbs   BSA   AFB$_1$

its excellent superiority, the EC immunosensor has been widely applied for mycotoxin detection in different matrices.[26−28]

To further improve the detection sensitivity and enhance the analytical performance of the EC immunosensor, various nanomaterials are commonly introduced to modify the electrode surface for accelerating the charge transfer and improving the catalytic activity.[29,30] Among them, multiwall carbon nanotubes (MWCNTs), a kind of hollow and multilayer nanomaterials with a special SP^2 hybrid structure,[31,32] exhibit a large specific surface area, excellent conductivity, strong catalytic activity, and good biocompatibility, which can be utilized in the EC immunosensing platform to achieve remarkable electrical signal amplification for the ultrasensitive detection of trace mycotoxins. What's more, MWCNTs modified with some functional groups are beneficial for uploading more recognition elements such as Abs to improve the detection specificity and sensitivity.[33] For example, the carboxylation functionalization can shorten the length of MWCNTs and introduce numerous carboxyl (−COOH) groups on the surface to significantly improve their dispersibility in water and provide sufficient active sites for binding with abundant Abs to capture targets. In addition, the functionalized MWCNTs need to be steadily uploaded onto the surface of the Au electrode to fabricate a stable EC immunosensor. Nafion with excellent film-forming ability and cation exchange characteristics is frequently introduced to assemble or carry functionalized MWCNTs to enhance their mechanical strength and stability and further improve the analytical performance of the established EC immunosensor.

Therefore, in this study, an ultrasensitive EC immunosensor with Nafion-immobilized functionalized MWCNTs for electrical signal amplification was developed for the trace detection of AFB$_1$ (Scheme 1). First, the functionalized MWCNTs were assembled and tightly fixed on the surface of a reusable Au electrode through the high adhesion ability of the Nafion film. Then, the EDC/NHS mixed solution was dropped to sufficiently activate the carboxyl (−COOH) groups of MWCNTs for the good immobilization of anti-AFB$_1$ Abs. Bovine serum albumin (BSA) was used to block the nonspecific binding sites. In the presence of AFB$_1$, it was specifically recognized and captured by anti-AFB$_1$ Abs, reducing the amplified current signals, which were recorded by cyclic voltammetry (CV) and differential pulse voltammetry (DPV) methods for accurate quantitation of AFB$_1$. Because of the synergistic effects of Nafion for stabilizing functionalized MWCNTs as signal enhancers and mAbs with high recognition ability, the developed EC immunosensor exhibited merits of easy construction, low cost, good reusability, and environmental friendliness, as well as high selectivity, excellent sensitivity, good stability, and good accuracy for AFB$_1$ detection in real malt, lotus seed, and Hirudo samples, demonstrating a broad application prospect in foods and more complex matrices.

■ MATERIALS AND METHODS

Materials and Apparatus. Malt and lotus seed samples were purchased from Beijing Tongrentang (Beijing, China). Hirudo samples were purchased from Chongqing Duoputai Pharmaceutical Co. Ltd. (Chongqing, China). 1-Ethyl-3-(3-
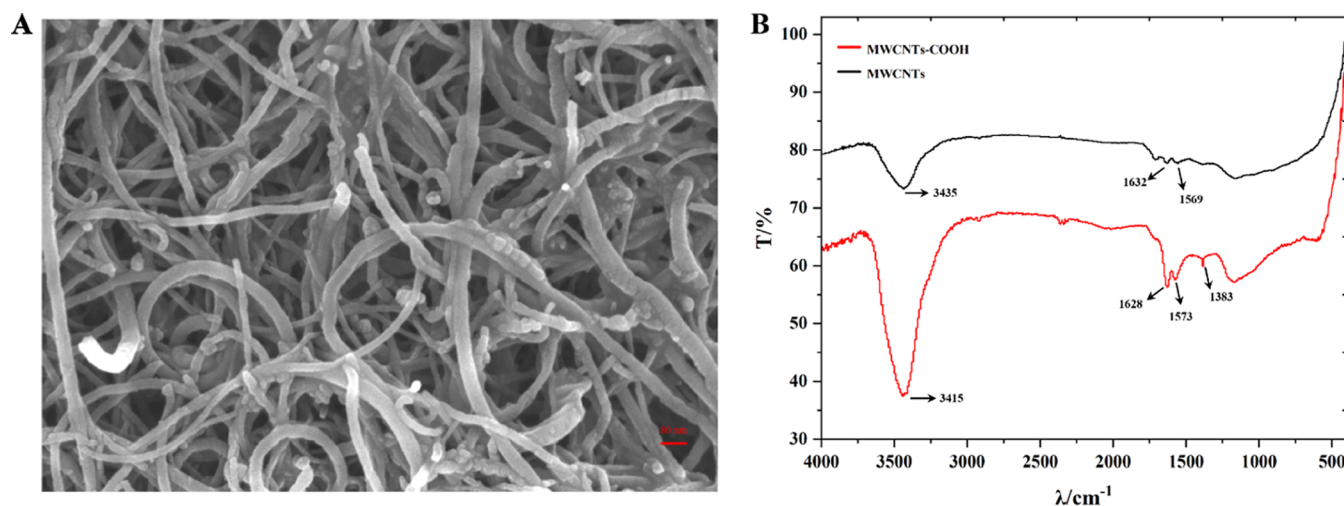
Figure 1. (A) SEM image and (B) FTIR spectrum of the functionalized MWCNTs.

(dimethylamino)propyl) carbodiimide hydrochloride (EDC), N-hydroxysuccinimide (NHS), potassium ferri cyanide ($K_3Fe(CN)_6$), hydrogen peroxide (30%), and sulfuric acid were all obtained from Sigma-Aldrich, France. AFB_1, ochratoxin A (OTA), zearalenone (ZEN), deoxynivalenol (DON) standard solution, and murine mAbs of AFB_1 (anti-AFB_1, 4.5 mg/mL, stored in PBS solution at −20 °C) were all bought from Shandong Lvdu Bioscience & Technology Co. Ltd. (Shandong, China). Multiwall carbon nanotubes (MWCNTs) and bovine serum albumin (BSA) were purchased from Aladdin Shanghai, China. 0.01 M PBS (pH 7.4) solution was prepared by dissolving 0.01 M Na_2HPO_4, 0.01 M KH_2PO_4, 4 g of NaCl, and 0.1 g of KCl in 500 mL of water with the pH adjusted to 7.4 by using HCl.

A CHI760E electrochemical workstation from Chenhua Instrument Co. Ltd. (Shanghai, China) was applied for all measurements. An iS10 FTIR spectrometer from Thermo Nicolet Corporation and a Hitachi S-4800 from Hitachi Limited (Japan) were applied for the characterization of MWCNTs.

Preparation of the Standard and Sample Solutions. AFB_1, OTA, ZEN, and DON standard solutions (1 mg/mL for each mycotoxin) were dissolved with PBS (pH 7.4), respectively, to prepare different concentrations of the working solution, which were all stored at −20 °C until use.

Malt, lotus seed, and Hirudo samples were ground to fine powders, respectively. Each group of sample powder was added with AFB_1 or the mixed solution of other mycotoxins containing ZEN, OTA, and DON, followed by the addition of 5 mL of 80% methanol. The spiked samples were vortexed for 10 min to extract the target mycotoxins. The supernatant was collected, dried with nitrogen, and finally redissolved in PBS solution for actual analysis.

Functionalization of MWCNTs. The superior sensitivity of the EC immunosensor was mainly attributed to the signal amplification of MWCNTs, which also provided a large number of active sites for immobilizing anti-AFB_1 monoclonal Abs (mAbs). MWCNTs were added with concentrated nitric acid at a ratio of 1:200, and the mixed solution was heated and refluxed in an oil bath for 12 h for the introduction of abundant carboxyl groups. Then, the −COOH-functionalized MWCNTs were rinsed with ultrapure water to pH 7.0 for further use.

Fabrication of the EC Immunosensor. The construction process of the functionalized MWCNT-based EC immunosensor on the working electrode is presented in Scheme 1. First, the surface of Au electrode was sufficiently rubbed with 50 nm alumina slurry (Al_2O_3) powder, subsequently rinsed with ultrapure water, cleaned by ultrasonic treatment for 30 s, and then immersed in the piranha solution (30% H_2O_2/H_2SO_4 = 1:3) for 3 min to purify the electrode surface, and the sample was rinsed thoroughly with ultrapure water. Then, 4 μL of the functionalized MWCNT solution was added onto the clean surface of the Au working electrode and dried at 37 °C. Then, 3 μL of Nafion solution was dropped onto the modified electrode surface and dried at room temperature for 5 min to adhere and fix functionalized MWCNTs. The Au/MWCNTs/Nafion electrode was then immersed in 60 μL of crosslinker solution containing 0.02 M EDC and 0.01 M NHS for 20 min at room temperature. After rinsing with ultrapure water, the modified working electrode was incubated in 60 μL of anti-AFB_1 mAbs solution for 1 h at 24 °C. Subsequently, the Au/MWCNT/Nafion/mAbs electrode was immersed in 60 μL of 1% BSA solution for 20 min at 24 °C to block the nonspecific binding sites of −COOH-functionalized MWCNTs, followed by rinsing with ultrapure water. Finally, the prepared MWCNTs/Nafion/mAbs/BSA-modified Au electrode was incubated with 60 μL of different concentrations of AFB_1 standard solution for 1.5 h at 24 °C, which, after rinsing thoroughly with ultrapure water, was subjected to CV and DPV measurements.

EC Detection of AFB_1. A conventional three-electrode system was used for the EC immunosensing of AFB_1. The decorated Au electrode was regarded as the working electrode, a saturated calomel electrode (SCE) was regarded as the reference electrode, and a platinum wire was regarded as the auxiliary electrode. The modified electrode was measured by CV and DPV methods in 5 mM $K_3[Fe(CN)_6]$ containing 0.4 M KNO_3. CV detection conditions were as follows: scan range: −0.3 to +0.7 V; interval: 0.001 V; scan rate: 0.05 V/s. DPV detection parameters were as follows: scan range: −0.3 to +0.4 V; pulse period: 0.5 s; pulse amplitude: 50 mV; and interval time: 0.0167 s.

Under the optimum conditions, the conductivity and EC signals of the modified Au electrode decreased with increasing AFB_1 concentration because of the strong steric resistance and
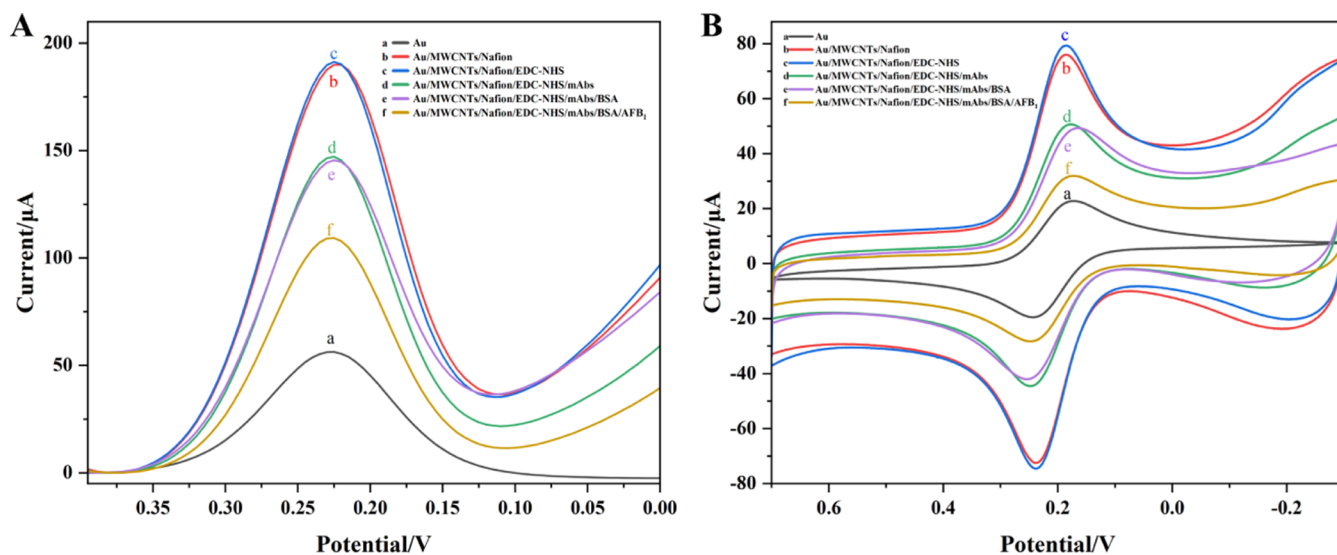
Figure 2. (A) DPV and (B) CV curves of the (a) bare Au electrode, (b) Au/MWCNTs/Nafion, (c) Au/MWCNTs/Nafion/EDC-NHS, (d) Au/MWCNTs/Nafion/EDC-NHS/mAbs, (e) Au/MWCNTs/Nafion/EDC-NHS/mAbs/BSA, and (f) Au/MWCNTs/Nafion/EDC-NHS/mAbs/BSA/AFB$_1$ Ag in 5 mM K$_3$[Fe(CN)$_6$] solution.

nonconductivity of AFB$_1$, thus decreasing the current intensity (*I*), which was recorded for the quantitation of AFB$_1$ in real samples.

RESULTS AND DISCUSSION

Characterization of MWCNTs. The microstructure of functionalized MWCNTs was first characterized by using a scanning electron microscope (SEM). The SEM image in Figure 1A exhibits the curly distribution of MWCNTs with large specific surface areas and an external diameter of about 80 nm due to their unique structures.

Then, the groups of MWCNTs after surface-carboxyl functionalization were characterized by FTIR analysis. The FTIR spectra in Figure 1B indicate a significant −OH absorption peak of MWCNTs-COOH at 3415 cm^{-1} and C=O absorption peaks at 1628−1383 cm^{-1}, which verified the introduction of −COOH groups and the successful preparation of functionalized MWCNTs.

Characterization of the EC Immunosensor. Here, the stepwise fabrication of the functionalized MWCNT-based EC immunosensor regarding the modification of the Au working electrode was first characterized by recording the DPV signals. By using this method, the redox current signals of some impurities in real samples were eliminated by current subtraction, thus greatly reducing background interferences.

Figure 2A shows that the bare Au electrode (curve *a*) exhibited the lowest peak current intensity (*I*) of about 56 μA because of its poor electrical conductivity. When the functionalized MWCNTs were doped onto the surface of the bare Au electrode and fixed by Nafion, the peak current intensity (curve *b*) was remarkably increased to 190.26 μA because of the large surface area and excellent conductivity of MWCNTs. A further slight current signal enhancement (191.30 μA) was observed (curve *c*) when the EDC-NHS solution was introduced onto the modified Au electrode, which might be due to the accelerated electron transfer rate resulting from the intermediate formed by NHS and activated carboxyl groups of MWCNTs between the sensing interface and [Fe(CN)6]$^{3-/4-}$ during the carboxyl activation process. Thus, modification of the Au electrode by functionalized

MWCNTs could achieve prominent electrical signal amplification to enhance the detection sensitivity for AFB$_1$.

When the anti-AFB$_1$ mAbs were loaded onto the Au/MWCNTs/Nafion/EDC-NHS-modified electrode, a significant decrease in current intensity (147.15 μA) was induced (curve *d*) due to the insulation and nonconductivity properties of macromolecular Abs, which largely impeded the electron transfer on the sensing interface. Then, a further slight reduction (curve *e*) in the current intensity (145.52 μA) was observed after BSA was loaded to block the redundant binding sites, because of its insulation property. After the Au/MWCNTs/Nafion/EDC-NHS/mAbs/BSA-modified electrode was incubated with 60 μL of AFB$_1$ solution (5 ng/mL), the anti-AFB$_1$ mAbs specifically captured the target AFB$_1$ to form the mAbs-AFB$_1$ Ag conjugates, which exhibited a strong spatial impedance effect to inhibit the electron transfer between the sensing interface and [Fe(CN)6]$^{3-/4-}$, leading to a reduction of the current intensity to the largest extent (curve *f*). Each step of DPV characterization indicated the successful preparation of the modified working electrode and the fabrication of the functionalized MWCNT-based EC immunosensor.

CV is also a useful method to measure the electrical potential difference between the oxidation and reduction peaks as well as the peak current of the oxidation−reduction curve to evaluate the performance of the modified Au electrode. Herein, the CV technique is also used to further verify the fabrication of the EC immunosensor. As shown in Figure 2B, a similar trend in each step was observed with respect to the findings in DPV measurements, further confirming the successful construction of the functionalized MWCNT-based EC immunosensor.

Optimization of the Fabrication Conditions for the EC Immunosensor. To achieve a stable and sensitive EC immunosensor with excellent performance for AFB$_1$ detection, some crucial conditions in modifying the Au working electrode to fabricate the EC immunosensor were optimized.

In this study, functionalized MWCNTs, with a large surface to mobilize abundant anti-AFB$_1$ mAbs and good conductivity to accelerate the electron transfer for improving the detection
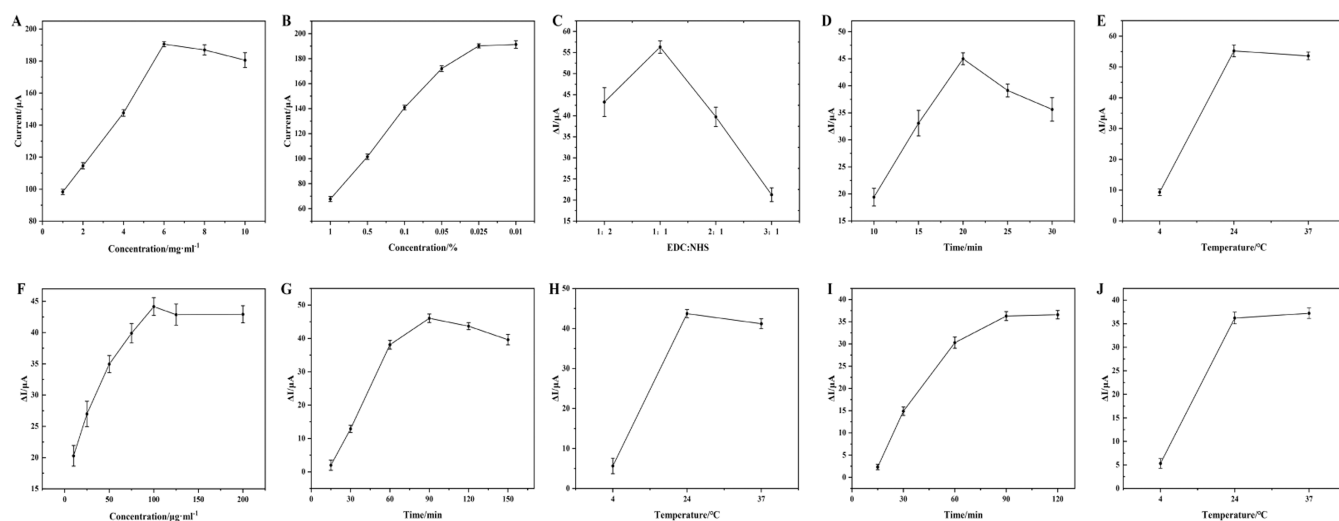
Figure 3. Optimization of the fabrication conditions for the EC immunosensor under different (A) concentrations of functionalized MWCNTs, (B) concentrations of Nafion solution, (C) proportions of EDC and NHS, (D) incubation times of EDC/NHS, (E) activation temperatures of EDC/NHS, (F) concentrations of anti-AFB$_1$ mAbs, (G) incubation times of anti-AFB$_1$ mAbs, (H) incubation temperatures of anti-AFB$_1$ mAbs, (I) incubation times of AFB$_1$, and (J) incubation temperatures of AFB$_1$.

sensitivity, were applied as the signal amplifiers to modify the Au working electrode, the added amount of which was thus extremely vital to realize high performance of the EC immunosensor. A very small amount of functionalized MWCNTs would not achieve sufficient amplification of the electrical signals, while at very high concentrations, they would accumulate and overlap on the electrode surface, causing an uneven distribution to lower the stability of the EC immunosensor. Here, 1−10 mg/mL functionalized MWCNTs were taken into consideration to modify the electrode surface. Figure 3A shows that the DPV current value continued to increase with increasing amounts of functionalized MWCNTs added in the range of 1−6 mg/mL and then declined when the concentration was more than 6 mg/mL. Thus, 6 mg/mL was regarded as the optimum added concentration of function-alized MWCNTs.

The added Nafion solution was vital to steadily immobilize the functionalized MWCNTs on the Au working electrode to construct a stable immunosensor. Nevertheless, due to its poor electrical conductivity, a large amount of Nafion solution used would hinder the electron transfer and lower the sensitivity of the immunosensor. Here, 0.01−1% Nafion solution in 95% alcohol (v/v) was considered to evaluate the conductivity of the functionalized MWCNT-decorated Au electrode and the changes in DPV signals. Figure 3B shows that the DPV current intensities of the Nafion-coated functionalized MWCNT-decorated Au electrode exhibit a slight decrease on increasing the added amount of Nafion from 0.01 to 0.025% and then rapidly decline. This indicated that when the added concentration of Nafion solution was 0.025%, the conductivity of the modified electrode was optimal, and functionalized MWCNTs were also firmly fixed.

EDC and NHS are commonly used as carboxyl activation reagents in amide synthesis. The carboxyl groups on the surface of MWCNTs are activated by EDC by forming active MWCNT-COO-acylosourea intermediates, which then react with NHS to form the MWCNTs-COO-NHS intermediates that are stable in PBS solution to promote the mAbs connection. The EDC/NHS activation efficiency influences the binding rate of mAbs at the sensing interface, thus affecting

the detection range and sensitivity of the EC immunosensor. High activation of the active groups with EDC/NHS is beneficial for binding with abundant mAbs to improve the detection sensitivity. To obtain the optimal activation efficiency, the concentration proportion, incubation time, and activation temperature of EDC/NHS solution were investigated by comparing the oxidation peak current difference (ΔI) before and after 50 ng/mL anti-AFB$_1$ mAbs was loaded onto the decorated Au electrode surface under different activation conditions in 5 mM K$_3$[Fe(CN)$_6$] solution. First, the proportion of EDC to NHS (1:2, 1:1, 2:1, and 3:1, v/v) was studied for the carboxyl activation of MWCNTs by the DPV method. As shown in Figure 3C, the ΔI values exhibited an increasing and then declining trend, and the maximum value (56.30 μA) was obtained at EDC/NHS = 1:1, which was regarded as the optimum proportion of EDC to NHS. In addition, an appropriate time of EDC/NHS activation is beneficial, as a very short time will lead to incomplete activation of the carboxyl groups, and long-time activation may cause the partial degradation of MWCNTs-COO-NHS intermediates, thus inducing a decrease in the binding rate of anti-AFB$_1$ mAbs. Therefore, the EDC/NHS activation within 10−30 min was investigated. Figure 3D indicates that the ΔI values continuously increased and reached the top at 20 min and then decreased. Thus, the EDC/NHS activation reaction for the carboxyl groups of MWCNTs was controlled within 20 min. Finally, in order to achieve the optimal effect, the EDC/NHS activation reaction would be controlled at a suitable temperature (4, 24, or 37 °C). As shown in Figure 3E, the highest ΔI value was obtained when the EDC/NHS activation reaction was set at 24 °C (room temperature). Under the optimized conditions, the carboxyl groups of MWCNTs could reach the best activation efficiency with EDC/NHS (1:1, v/v) at 24 °C for 20 min, which would benefit the recognition and capture of enough anti-AFB$_1$ mAbs through the amide reaction to improve the detection sensitivity of the immunosensor for AFB$_1$.

The pivotal recognition elements, anti-AFB$_1$ mAbs immo-bilized on the functionalized MWCNTs, were directly relevant to the binding amount of the target AFB$_1$ through the Ag−Ab
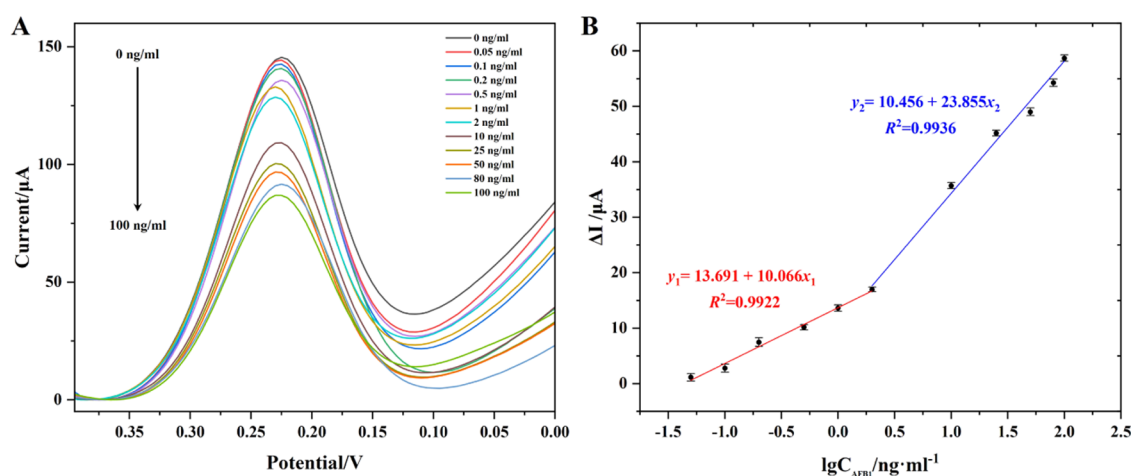
Figure 4. (A) DPV peak current for different concentrations (0−100 ng/mL) of AFB$_1$, and (B) the calibration curve between ΔI and the logarithm of AFB$_1$ concentration by using the developed EC immunosensor (n = 3).

Table 1. Comparison of the As-Prepared AFB$_1$ Immunosensors with Other Reported Sensors for the Detection of AFB$_1$

electrode material	method	linear range (ng/mL)	LOD (ng/mL)	refs
Au/CdS@PDA/WO$_3$	DPV	10−20,000	0.94	34
Au/PEI/CNFs	DPV	0.05−20	0.027	35
PAN/ZnO/APTES/GA	PL	0.1−20	0.039	36
AuNFs/AFB$_1$-Apt/Cy$_3$	DPV	0.1−100	0.014	37
Au$_8$NC-PSMA/mAbs	fluorescent immunoassay	0−20	0.27	38
Cu$_{2−x}$Se−Au-mAbs	thermal analysis	10−10,000	8.42	39
Au/MWCNTs/Nafion/mAbs/BSA	DPV	0.05−100	0.021	this work

reaction. Therefore, the added amount of anti-AFB$_1$ mAbs, along with their incubation time and temperature, were regarded as the important parameters, which were systematically investigated by the DPV method in 5 mM K$_3$[Fe(CN)$_6$] solution. The added amount of anti-AFB$_1$ mAbs is extremely crucial to realize a high sensitivity and wide detection range of the immunosensor. A very small amount of anti-AFB$_1$ mAbs will lead to incomplete binding of target AFB$_1$ in samples, while a very high concentration would result in large wastage. Figure 3F shows that with increasing concentration of added anti-AFB$_1$ mAbs in the range of 10−200 μg/mL, the ΔI (before and after anti-AFB$_1$ mAbs connection) increased and then declined. When the anti-AFB$_1$ mAbs concentration reached 100 μg/mL, the highest ΔI value (44.15 μA) was obtained, which was selected as the optimum added concentration of anti-AFB$_1$ mAbs. It is known that sufficient incubation time at a suitable temperature can ensure the maximum connection of the anti-AFB$_1$ mAbs. Thus, the incubation time of anti-AFB$_1$ mAbs was analyzed in the range of 15−150 min. Figure 3G shows that ΔI reached the maximum value (46.04 μA) at 90 min. Regarding the incubation temperature, the highest value was observed at 24 °C (Figure 3H). Therefore, considering time and economic cost, 100 μg/mL anti-AFB$_1$ mAbs was uploaded onto the surface of the Nafion-immobilized functionalized MWCNT-decorated Au electrode for incubation for 60 min at 24 °C, which allowed the capture of a large number of AFB$_1$ molecules to enhance the detection sensitivity and specificity of the sensor for AFB$_1$ in complex samples.

After the Au/MWCNTs/Nafion/mAbs/BSA immunosensor was fabricated, the target AFB$_1$ in the standard and sample solutions was recognized by the specific mAbs on the sensor surface for its real determination. Thus, the incubation time

and temperature of AFB$_1$ with the immunosensor were investigated by the DPV method in 5 mM K$_3$[Fe(CN)$_6$] solution. It is noted that a very short incubation time will lead to incomplete Ag−Ab reaction, while incubation for a long time may cause the shedding of Ag due to the reversibility of the coupling reaction. Figure 3I illustrates that on prolonging the incubation time of AFB$_1$ on the fabricated immunosensor from 15 to 90 min, the ΔI value (before and after AFB$_1$ connection with anti-AFB$_1$ mAbs) increased significantly and reached the highest value (36.58 μA) when the incubation time reached 90 min, which was selected as the optimum incubation time of AFB$_1$ or the test sample containing AFB$_1$ on the decorated Au electrode. Regarding the incubation temperature, Figure 3J shows that the highest ΔI value was observed when the incubation temperature was set at 37 °C. In summary, after the sample solution was dropped onto the sensor at 37 °C for incubation for 90 min, quantitative analysis of the target AFB$_1$ could be achieved.

Analytical Performance of the Developed EC Immunosensor. After the construction of the Nafion-immobilized functionalized MWCNT-based immunosensor, a series of concentrations of AFB$_1$ solution was added to measure the changed DPV responses under the optimized conditions.

Figure 4A shows that the DPV current signals decreased with an increase in the added concentration of AFB$_1$ in the range of 0−100 ng/mL, which were inversely proportional to the AFB$_1$ concentration. Figure 4B shows that the developed immunosensor exhibited an excellent linear relationship between the changed DPV current intensity (ΔI) and the logarithm of AFB$_1$ concentration (x) from 0.05 to 100 ng/mL, yielding two calibration curves within the low and high concentration ranges: y_1 = 10.066 x_1 + 13.691 (0.05−2 ng/mL,

$R^2 = 0.9922$) and $y_2 = 23.855 x_2 + 10.456$ (2−100 ng/mL, $R^2 = 0.9936$). The limit of detection (LOD) was as low as 0.021 ng/mL. Compared with other reported sensors for the detection of AFB_1 (Table 1), the newly developed Au/MWCNT/Nafion/mAbs/BSA immunosensor exhibited a much lower LOD and a wider linear range, demonstrating its excellent ability for trace AFB_1 detection in real food samples.

Good specificity with strong anti-interference ability was crucial regarding the developed immunosensor, which, herein, is investigated by incubating $1 \times$ PBS (pH 7.4) blank solution, 1 ng/mL AFB_1, and three interfering mycotoxins of ZEN, OTA, and DON (100 ng/mL), respectively, under the same conditions. Figure 5 shows that the ΔI values resulting from
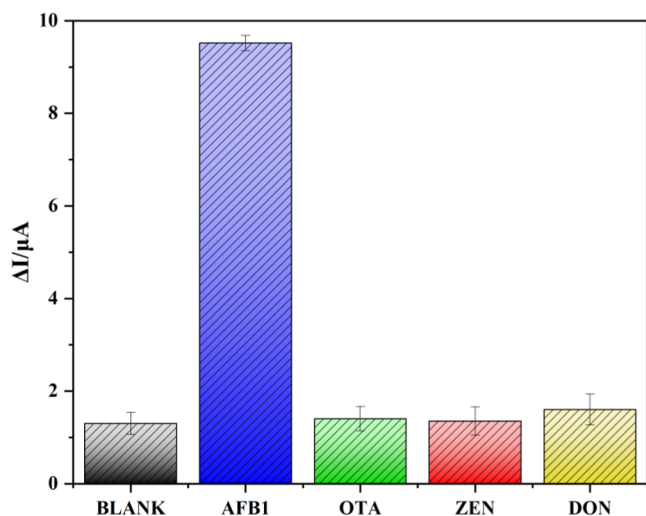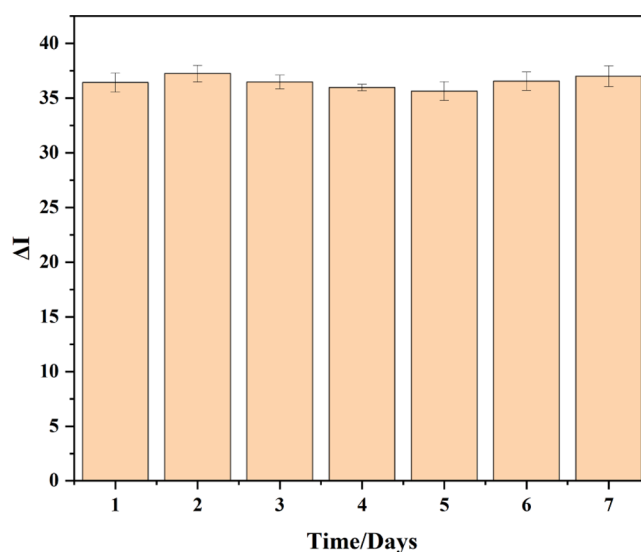

Figure 5. Change in DPV current intensities of the as-prepared immunosensors with the addition of the blank solution ($1 \times$ PBS, pH 7.4), 1 ng/mL AFB_1, and 100 ng/mL OTA, ZEN, and DON in $1 \times$ PBS solution (pH 7.4).

the addition of 100 ng/mL ZEN, OTA, and DON were almost the same as that with the PBS solution. However, the introduction of 1 ng/mL AFB_1 induced remarkably increased (almost 9-fold) ΔI values in comparison with the blank solution and other mycotoxins, indicating that the addition of an ultralow level (1 ng/mL) of AFB_1 caused significant current changes, while no change in DPV current was observed upon the addition of other interferences with a concentration 100-fold that of target AFB_1. These verified the high specificity and anti-interference ability of the newly developed immunosensor toward AFB_1.

In order to evaluate the stability of the developed immunosensor, the prepared Au/MWCNT/Nafion/mAbs/BSA electrode was stored in $1 \times$ PBS (pH 7.4) solution at 4 °C for 7 days, followed by measurement through the DPV method after incubation with 10 ng/mL AFB_1 solution. The result showed that the DPV currents measured every day were stable, with the relative standard deviation (RSD) < 3.26% ($n = 3$), indicating the good stability of the Nafion-immobilized functionalized MWCNT-based immunosensor within 7 days (Figure 6).

Real Sample Analysis for AFB_1. The accuracy and practicability of the newly developed immunosensor were verified in real samples by using the standard addition method for AFB_1 detection. Malt, lotus seed, and hirudo samples that were confirmed to be without AFB_1 residue were fortified with

Figure 6. Change in DPV current intensities of the developed immunosensor in a $1 \times$ PBS (pH 7.4) solution at 4 °C.

different concentrations (5, 20, and 80 ng/mL) of AFB_1 standard solution, followed by the above-presented procedure for sample preparation, AFB_1 extraction, and detection by using the developed immunosensor. Each spiked sample was tested five times ($n = 5$), and the recovery (%) was calculated as the ratio of the measured amount by the immunosensor to the actually added amount of AFB_1. Table 2 displays that the

Table 2. Recovery of AFB_1 in the Spiked Samples ($n = 5$)

samples	added amount (ng/mL)	measured amount (ng/mL)	recovery (%)	RSD (%)
malt	5	4.707	94.14	2.41
	20	19.498	97.49	2.32
	80	81.982	102.48	2.73
lotus seed	5	4.793	95.86	2.58
	20	19.682	98.41	2.64
	80	81.930	102.41	2.09
hirudo	5	4.604	92.08	2.73
	20	20.923	104.62	3.42
	80	83.680	104.60	3.06

recovery values for the three tested samples are in the range of 92.08−104.62% with RSD < 3.42%, which were 94.14−102.48% with RSD < 2.73% for the spiked malt samples, 95.86−102.41% with RSD < 2.64% for the fortified lotus seed samples, and 92.08−104.62% with RSD < 3.42% for the spiked hirudo samples. All of the obtained recovery and RSD data were acceptable and satisfactory, indicating the excellent feasibility, accuracy, and applicability of the developed aptasensor for the precision quantitation of AFB_1 in real complex food matrices. In the future, the developed immunesensor can be combined with a smartphone platform[26,40] to achieve more convenient onsite detection of more trace mycotoxins in complex matrices.

■ CONCLUSIONS

In this study, a simple-to-construct, easy-to-operate, and ultrasensitive Nafion-immobilized functionalized MWCNT-based immunosensor with excellent selectivity and stability was successfully developed for trace AFB_1 detection in complex

matrices. The introduced Nafion film could steadily immobilize functionalized MWCNTs with uniform distribution and tiling on the surface of the Au electrode. Functionalized MWCNTs with a large specific surface area and abundant active sites to couple with numerous anti-AFB$_1$ mAbs, good conductivity, and high catalytic activity to serve as the signal amplifier were immobilized with the Nafion film to be utilized as the substrate for remarkably enhancing the sensing performance of the immunosensor. All of these endowed the functionalized MWCNTs amplification strategy-based EC immunosensor with superior merits such as high selectivity, excellent sensitivity with a low LOD of 0.021 ng/mL, a wide detection range of 0.05−100 ng/mL, and satisfactory accuracy with a recovery of 92.08−104.62% in the complex malt, lotus seed, and hirudo samples. Thus, it exhibits broad application prospects in food safety, environmental pollution monitoring, clinical analysis, and other fields.

■ AUTHOR INFORMATION

Corresponding Author

Li Ma − School of Traditional Chinese Medicine, Capital Medical University, Beijing 100069, China; orcid.org/0000-0002-5915-7147; Email: marytcm@ccmu.edu.cn

Authors

Kai Deng − School of Traditional Chinese Medicine, Capital Medical University, Beijing 100069, China; Laboratory for Clinical Medicine, Capital Medical University, Beijing 100069, China

Yining Zhang − School of Traditional Chinese Medicine, Capital Medical University, Beijing 100069, China; Laboratory for Clinical Medicine, Capital Medical University, Beijing 100069, China

Hang Xiao − School of Traditional Chinese Medicine, Capital Medical University, Beijing 100069, China

Yujiao Hou − Institute of Medicinal Plant Development, Chinese Academy of Medical Sciences and Peking Union Medical College, Beijing 100193, China

Qingbin Xu − Institute of Medicinal Plant Development, Chinese Academy of Medical Sciences and Peking Union Medical College, Beijing 100193, China

Ying Li − Institute of Medicinal Plant Development, Chinese Academy of Medical Sciences and Peking Union Medical College, Beijing 100193, China

Weijun Kong − School of Traditional Chinese Medicine, Capital Medical University, Beijing 100069, China; Laboratory for Clinical Medicine, Capital Medical University, Beijing 100069, China; orcid.org/0000-0001-9943-7218

Complete contact information is available at:
https://pubs.acs.org/10.1021/acsomega.3c04619

Author Contributions

$^{\parallel}$K.D. and Y.Z. contributed equally to this work and should be regarded as co-first authors. **K.D.:** formal analysis and writing—original draft. **Y.Z.:** formal analysis and writing—original draft. **H.X.:** formal analysis. **Y.H.:** resources and methodology. **Q.X.:** formal analysis. **Y.L.:** validation and investigation. **W.K.:** conceptualization, supervision, writing—review and editing, supervision, and funding acquisition. **L.M.:** conceptualization, supervision, and funding acquisition.

Notes

The authors declare no competing financial interest.

■ REFERENCES

(1) Caceres, I.; Khoury, A. A.; Khoury, R. E.; Lorber, S.; Oswald, I. P.; Khoury, A. E.; Atoui, A.; Puel, O.; Bailly, J. D. Aflatoxin biosynthesis and genetic regulation: A review. *Toxins* **2020**, *12*, 150.

(2) Shabeer, S.; Asad, S.; Jamal, A.; Ali, A. Aflatoxin contamination, its impact and management strategies: An updated review. *Toxins* **2022**, *14*, 307.

(3) Benkerroum, N. Chronic and acute toxicities of aflatoxins: Mechanisms of action. *Int. J. Environ. Res. Public Health* **2020**, *17*, 423−451.

(4) Pickova, D.; Ostry, V.; Toman, J.; Malir, F. Aflatoxins: History, significant milestones, recent data on their toxicity and ways to mitigation. *Toxins* **2021**, *13*, 399.

(5) Cao, P.; Wang, G.; Wei, X. M.; Chen, S. L.; Han, J. P. How to improve CHMs quality: Enlighten from CHMs ecological cultivation. *Chin. Herb. Med.* **2021**, *13*, 301−312.

(6) Jallow, A.; Xie, H. L.; Tang, X. Q.; Qi, Z.; Li, P. W. Worldwide aflatoxin contamination of agricultural products and foods: From occurrence to control. *Compr. Rev. Food Sci. Food Saf.* **2021**, *20*, 2332−2381.

(7) Patyal, A.; Gill, J.; Bedi, J. S.; Aulakh, R. S. Assessment of aflatoxin contamination in dairy animal concentrate feed from Punjab, India. *Environ. Sci. Pollut. Res. Int.* **2021**, *28*, 37705−37715.

(8) Rushing, B. R.; Selim, M. I. Aflatoxin B$_1$: A review on metabolism, toxicity, occurrence in food, occupational exposure, and detoxification methods. *Food Chem. Toxicol.* **2019**, *124*, 81−100.

(9) Chen, Y. Y.; Li, R. R.; Chang, Q. C.; Dong, Z. H.; Yang, H. M.; Xu, C. Lactobacillus bulgaricus or lactobacillus rhamnosus suppresses NF-kappaB signaling pathway and protects against AFB$_1$-induced hepatitis: A novel potential preventive strategy for Aflatoxicosis? *Toxins* **2019**, *11*, 17.

(10) Ghallab, A.; Hassan, R.; Myllys, M.; Albrecht, W.; Friebel, A.; Hoehme, S.; Hofmann, U.; Seddek, A. L.; Braeuning, A.; Kuepfer, L.; Cramer, B.; Humpf, H. U.; Boor, P.; Degen, G. H.; Hengstler, J. G. Subcellular spatio-temporal intravital kinetics of aflatoxin B$_1$ and ochratoxin A in liver and kidney. *Arch. Toxicol.* **2021**, *95*, 2163−2177.

(11) McMillan, A.; Renaud, J. B.; Burgess, K.; Orimadegun, A. E.; Akinyinka, O. O.; Allen, S. J.; Miller, J. D.; Reid, G.; Sumarah, M. W. Aflatoxin exposure in nigerian children with severe acute malnutrition. *Food Chem. Toxicol.* **2018**, *111*, 356−362.

(12) Cao, W. Y.; Yu, P.; Yang, K. P.; Cao, D. L. Aflatoxin B$_1$: metabolism, toxicology, and its involvement in oxidative stress and cancer development. *Toxicol. Mech. Methods* **2022**, *32*, 395−419.

(13) Eaton, D. L.; Gallagher, E. P. Mechanisms of aflatoxin carcinogenesis. *Annu. Rev. Pharmacol. Toxicol.* **1994**, *34*, 135−172.

(14) Ekwomadu, T.; Mwanza, M.; Musekiwa, A. Mycotoxin-linked mutations and cancer risk: A global health issue. *Int. J. Environ. Res. Public Health* **2022**, *19*, 7754.

(15) Ajmal, M.; Bedale, W.; Akram, A.; Yu, J. H. Comprehensive review of aflatoxin contamination, impact on health and food security, and management strategies in Pakistan. *Toxins* **2022**, *14*, 845.

(16) Er Demirhan, B.; Demirhan, B. Investigation of twelve significant mycotoxin contamination in nut-based products by the LC-MS/MS method. *Metabolites* **2022**, *12*, 120.

(17) Xia, L.; Rasheed, H.; Routledge, M. N.; Wu, H.; Gong, Y. Y. Super-sensitive LC-MS analyses of exposure biomarkers for multiple mycotoxins in a rural pakistan population. *Toxins* **2022**, *14*, 193.

(18) Pantano, L.; La Scala, L.; Olibrio, F.; Galluzzo, F. G.; Bongiorno, C.; Buscemi, M. D.; Macaluso, A.; Vella, A. QuEChERS LC-MS/MS screening method for mycotoxin detection in cereal products and spices. *Int. J. Environ. Res. Public Health* **2021**, *18*, 3774.

(19) Salim, S. A.; Sukor, R.; Ismail, M. N.; Selamat, J. Dispersive liquid-liquid microextraction (DLLME) and LC-MS/MS analysis for multi-mycotoxin in rice bran: Method development,optimization and validation. *Toxins* **2021**, *13*, 280.

(20) Yu, Z. C.; Qiu, C. C.; Huang, L. T.; Gao, Y.; Tang, D. P. Microelectromechanical microsystems-supported photothermal immunoassay for point-of-care testing of aflatoxin B_1 in foodstuff. *Anal. Chem.* **2023**, *95*, 4212−4219.

(21) Tang, X. Q.; Catanante, G.; Huang, X. R.; Marty, J. L.; Wang, H.; Zhang, Q.; Li, P. W. Screen-printed electrochemical immunosensor based on a novel nanobody for analyzing aflatoxin M_1 in milk. *Food Chem.* **2022**, *383*, No. 132598.

(22) Malvano, F.; Pilloton, R.; Rubino, A.; Albanese, D. Rapid detection of deoxynivalenol in dry pasta using a label-free immunosensor. *Biosensors* **2022**, *12*, 240.

(23) Şenocak, A.; Sanko, V.; Tumay, S. O.; Orooji, Y.; Demirbas, E.; Yoon, Y.; Khataee, A. Ultrasensitive electrochemical sensor for detection of rutin antioxidant by layered $Ti_3Al_{0.5}Cu_{0.5}C_2$ MAX phase. *Food Chem. Toxicol.* **2022**, *164*, No. 113016.

(24) Nejadmansouri, M.; Majdinasab, M.; Nunes, G. S.; Marty, J. L. An overview of optical and electrochemical sensors and biosensors for analysis of antioxidants in food during the last 5 years. *Sensors* **2021**, *21*, 1176.

(25) Teymourian, H.; Parrilla, M.; Sempionatto, J. R.; Montiel, N. F.; Barfidokht, A.; Van Echelpoel, R.; DeWael, K.; Wang, J. Wearable electrochemical sensors for the monitoring and screening of drugs. *ACS Sens.* **2020**, *5*, 2679−2700.

(26) Jafari, S.; Burr, L.; Migliorelli, D.; Galve, R.; Marco, M. P.; Campbell, K.; Elliott, C.; Suman, M.; Sturla, S. J.; Generelli, S. Smartphone-based magneto-immunosensor on carbon black modified screen-printed electrodes for point-of-need detection of aflatoxin B_1 in cereals. *Anal. Chim. Acta* **2022**, *1221*, No. 340118.

(27) Pei, F. B.; Feng, S. S.; Zhang, Y. H.; Wu, Y.; Chen, C. L.; Sun, Y.; Xie, Z. H.; Hao, Q. L.; Cao, Y.; Tong, Z. Y.; Lei, W. A photoelectrochemical immunosensor based on Z-scheme CdS composite heterojunction for aflatoxin B_1. *Biosens. Bioelectron.* **2022**, *214*, No. 114500.

(28) Yuan, Z. H.; Dai, H.; Liu, X. D.; Duan, S.; Shen, Y. F.; Zhang, Q.; Shu, Z. X.; Xiao, A. H.; Wang, J. H. An electrochemical immunosensor based on prussian blue@zeolitic imidazolate framework-8 nanocomposites probe for the detection of deoxynivalenol in grain products. *Food Chem.* **2023**, *405*, No. 134842.

(29) Wordsworth, J.; Benedetti, T. M.; Somerville, S. V.; Schuhmann, W.; Tilley, R. D.; Gooding, J. J. The influence of nanoconfinement on electrocatalysis. *Angew. Chem., Int. Ed.* **2022**, *61*, No. e202200755.

(30) Adunphatcharaphon, S.; Elliott, C. T.; Sooksimuang, T.; Charlermroj, R.; Petchkongkaew, A.; Karoonuthaisiri, N. The evolution of multiplex detection of mycotoxins using immunoassay platform technologies. *J. Hazard. Mater.* **2022**, *432*, No. 128706.

(31) Escobar-Teran, F.; Perrot, H.; Sel, O. Ion dynamics at the carbon electrode/electrolyte interface: Influence of carbon nanotubes types. *Materials* **2022**, *15*, 1867.

(32) Du, X.; Li, Y. Y.; Zhang, Z. G.; Zhang, C. C.; Hu, J. C.; Wang, X. X.; Zhang, R. S.; Yang, J. L.; Zhou, L.; Zhang, H. Y.; Liu, M.; Zhou, J. An electrochemical biosensor for the assessment of tumor immunotherapy based on the detection of immune checkpoint protein programmed death ligand-1. *Biosens. Bioelectron.* **2022**, *207*, No. 114166.

(33) Xing, G. Q.; Luo, B.; Qin, J. Q.; Wang, X. D.; Hou, P. C.; Zhang, H.; Wang, C.; Wang, J. S.; Li, A. S. A probe-free electrochemical immunosensor for methyl jasmonate based on ferrocene functionalized-carboxylated graphene-multi-walled carbon nanotube nanocomposites. *Talanta* **2021**, *232*, No. 122477.

(34) Liu, B.; Peng, J. X.; Wu, Q. Y.; Zhao, Y. S.; Shang, H.; Wang, S. A novel screening on the specific peptide by molecular simulation and development of the electrochemical immunosensor for aflatoxin B_1 in grains. *Food Chem.* **2022**, *372*, No. 131322.

(35) Huang, Y. H.; Zhu, F.; Guan, J. H.; Wei, W.; Zou, L. Label-free amperometric immunosensor based on versatile carbon nanofibers network coupled with Au nanoparticles for Aflatoxin B_1 detection. *Biosensors* **2021**, *11*, 5.

(36) Myndrul, V.; Coy, E.; Bechelany, M.; Iatsunskyi, I. Photoluminescence label-free immunosensor for the detection of aflatoxin B_1 using polyacrylonitrile/zinc oxide nanofibers. *Mater. Sci. Eng. C* **2021**, *118*, No. 111401.

(37) Qiao, M. X.; Liu, Y.; Wei, M. Dual-signal output fluorescent aptasensor based on DNA programmability and gold nanoflowers for multiple mycotoxins detection. *Anal. Bioanal. Chem.* **2023**, *415*, 277−288.

(38) Shao, Z. H.; Zhai, A.; Hua, Y.; Mo, H. L.; Xie, F.; Zhao, X.; Zhao, G.; Zang, S. Q. Development of Au_8 nanocluster-based fluorescent strip immunosensor for sensitive detection of aflatoxin B_1. *Anal. Chim. Acta* **2023**, *1274*, No. 341576.

(39) Wang, Q.; Li, S.; Zhang, Y.; Wang, S.; Guo, J.; Wang, J. A highly sensitive photothermal immunochromatographic sensor for detection of aflatoxin B_1 based on $Cu_{2-x}Se$-Au nanoparticles. *Food Chem.* **2023**, *401*, No. 134065.

(40) Zuo, J.; Yan, T.; Tang, X.; Zhang, Q.; Li, P. Dual-Modal immunosensor made with the multifunction nanobody for fluorescent/colorimetric sensitive detection of Aflatoxin B_1 in maize. *ACS Appl. Mater. Interfaces* **2023**, *15*, 2771−2780.